

NRL Report 7737

Properties of RF Sputtered Zinc Oxide Thin Films for Microwave Acoustic Devices

T. R. LARSON AND M. FINNLEY

*Microwave Techniques Branch
Electronics Division*

May 1, 1974



NAVAL RESEARCH LABORATORY
Washington, D.C.

Approved for public release; distribution unlimited.

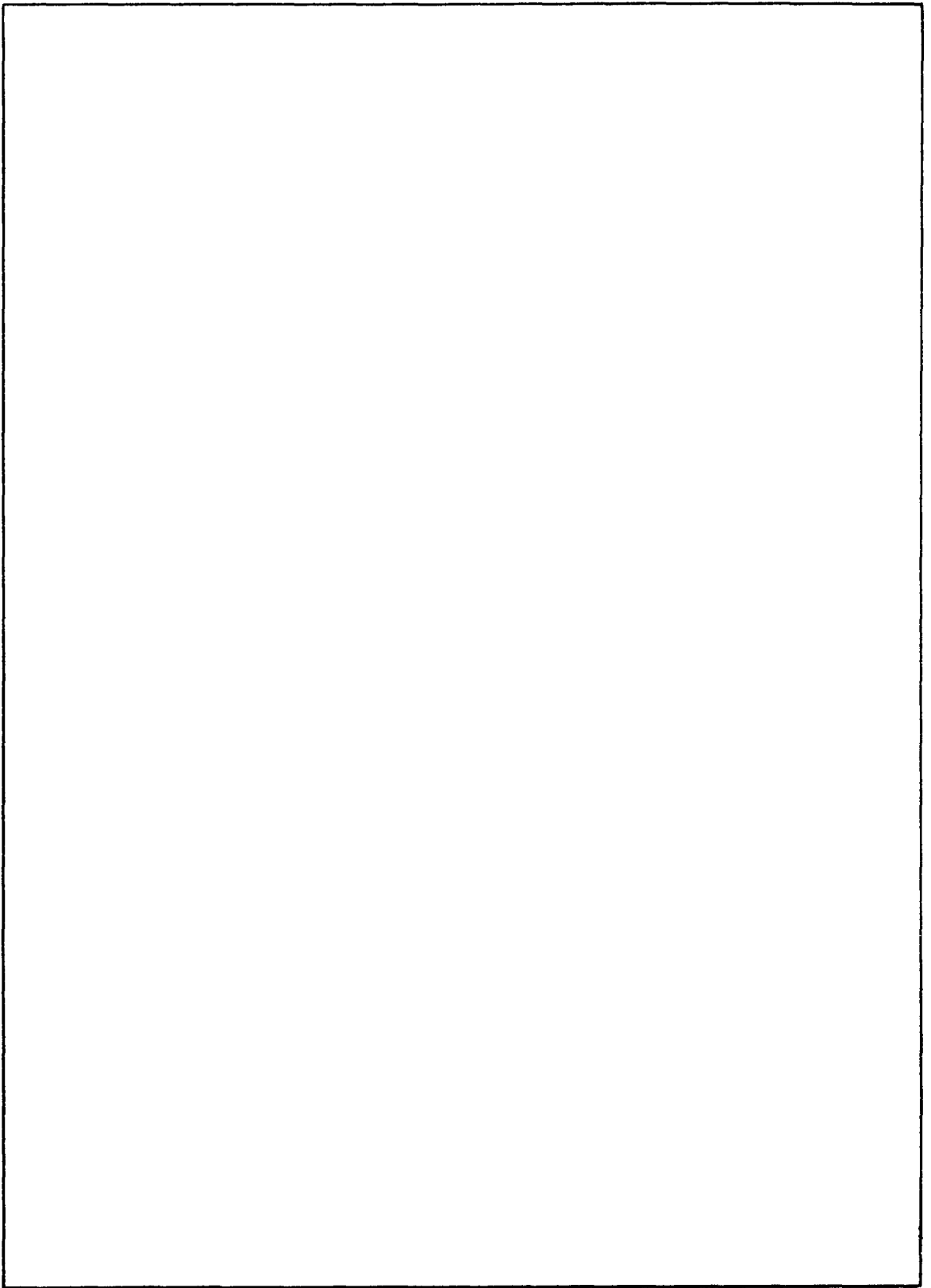
SECURITY CLASSIFICATION OF THIS PAGE (When Data Entered)

REPORT DOCUMENTATION PAGE		READ INSTRUCTIONS BEFORE COMPLETING FORM	
1. REPORT NUMBER NRL Report 7737	2. GOVT ACCESSION NO.	3. RECIPIENT'S CATALOG NUMBER	
4. TITLE (and Subtitle) PROPERTIES OF RF SPUTTERED ZINC OXIDE THIN FILMS FOR MICROWAVE ACOUSTIC DEVICES		5. TYPE OF REPORT & PERIOD COVERED Interim report on a continuing NRL Problem.	
		6. PERFORMING ORG. REPORT NUMBER	
7. AUTHOR(s) T. R. Larson, and M. Finnley		8. CONTRACT OR GRANT NUMBER(s)	
9. PERFORMING ORGANIZATION NAME AND ADDRESS Naval Research Laboratory Washington, D. C. 20375		10. PROGRAM ELEMENT, PROJECT, TASK AREA & WORK UNIT NUMBERS NRL Problem R08-54 RR021-05-41-5702	
11. CONTROLLING OFFICE NAME AND ADDRESS Department of the Navy Office of Naval Research Arlington, Va. 22217		12. REPORT DATE May 1, 1974	
		13. NUMBER OF PAGES 24	
14. MONITORING AGENCY NAME & ADDRESS (if different from Controlling Office)		15. SECURITY CLASS. (of this report) Unclassified	
		15a. DECLASSIFICATION/DOWNGRADING SCHEDULE	
16. DISTRIBUTION STATEMENT (of this Report) Approved for public release; distribution unlimited.			
17. DISTRIBUTION STATEMENT (of the abstract entered in Block 20, if different from Report)			
18. SUPPLEMENTARY NOTES			
19. KEY WORDS (Continue on reverse side if necessary and identify by block number) Surface acoustic waves Acoustic transducer Ultrasonic transducer Microwave acoustic device			
20. ABSTRACT (Continue on reverse side if necessary and identify by block number) Various factors involved in the production of piezoelectric zinc oxide thin films and their utilization as acoustic transducers were studied, along with techniques for analysis and fabrication of actual devices. The best transducers in this study exhibited coupling constants approximately 60% as large as the theoretical value and a minimum untuned insertion loss of 30 dB. Bulk transducer technology was emphasized, since analysis of the zinc oxide film is relatively easy in this configuration; however, most of the concepts are directly applicable to surface wave transducers, the ultimate motivation for this work.			

DD FORM 1473
1 JAN 73EDITION OF 1 NOV 65 IS OBSOLETE
S/N 0102-014-6601

i

SECURITY CLASSIFICATION OF THIS PAGE (When Data Entered)



CONTENTS

INTRODUCTION	1
ZnO FILMS: PROPERTIES AND ANALYTICAL TECHNIQUES	1
Electromechanical Coupling Coefficient	1
Resistivity	2
Optical Quality	2
Microstructure, SEM Photographs	2
Electron Diffraction	3
X-Ray Analysis	3
BULK WAVE TRANSDUCER ANALYSIS	7
TECHNIQUES	12
RESULTS AND PROBLEMS	15
FUTURE OUTLOOK	20
ACKNOWLEDGMENTS	21
REFERENCES	21

PROPERTIES OF RF SPUTTERED ZINC OXIDE THIN FILMS FOR MICROWAVE ACOUSTIC DEVICES

INTRODUCTION

Piezoelectric acoustic bulk wave transducers operating at microwave frequencies have been extensively studied [1-7]. Their main use is in acoustic delay lines for radar applications, computers, and signal processing. Because the sound velocity is of the order of 10^5 cm/s, piezoelectric layers one-half wavelength thick (the usual configuration), at a frequency of 1 GHz and above, must be about $1\ \mu\text{m}$ thick or less. In this thickness range, growing the piezoelectric film directly on a substrate (in this case using the RF sputtering technique) is the most practical fabrication method. The choice of material for this piezoelectric layer is governed largely by its gain-bandwidth product which is proportional to k^2 , where $0 < k < 1$ is the electroacoustic coupling coefficient. Zinc oxide single crystals have $k = 0.28$ (for longitudinal waves propagating along the c axis), and zinc oxide films have exhibited the largest k to date (the film k usually is not equal to the bulk value). Acoustic Surface Wave (ASW) overlay transducers, the long-range goal of this study, share many of the same piezoelectric film requirements as bulk transducers.

This report summarizes bulk wave transducer technology and includes device performance and fabrication techniques learned in about 60 runs, made over a period of 6 months, in a study of zinc oxide piezoelectric film growth. Although the background and analysis of ASW overlay transducers is not covered thoroughly, the performance of one such transducer, fabricated using experience gained from bulk wave transducer studies, is discussed.

ZnO FILMS: PROPERTIES AND ANALYTICAL TECHNIQUES

Bulk single crystal zinc oxide (ZnO) is a strong piezoelectric semiconductor with an electromechanical coupling coefficient $k = 0.28$ for bulk longitudinal acoustic waves propagating along the c axis of its Wurtzite lattice. With a band gap of 3.2 eV (3850 Å light), it is colorless and transparent. A discussion of the properties of ZnO thin films (not always the same as single crystal ZnO) and the techniques used to determine them is presented in the following sections.

Electromechanical Coupling Coefficient

If a ZnO film is to be used as a transducer, the quality of the film (i.e. how well it converts electrical energy into acoustic energy) is of vital importance. The parameter that represents this is the electromechanical coupling constant (k). It is also found that the

Note: Manuscript submitted February 20, 1974.

the gain-bandwidth product of any transducer scales directly with k^2 . An amorphous or randomly oriented film cannot exhibit macroscopic piezoelectric behavior, because the crystal axes do not exhibit the required reflection symmetry. Thus for a nonzero k , a film must be oriented to some extent. For longitudinal bulk wave transducers, the RF field is applied parallel to the c axis of the film and normal to the film plane. Thus only one piezoelectric coefficient (piezoelectricity is normally a tensor property) is used, and the only requirement is that the c axis of the film be normal to the film plane. The structure of most grown films seems to exhibit this orientation, consisting of many microscopic crystallites, with normal c axes but random basal plane axes [8].

Shear wave transducers require c axes either in the film plane or oriented at a fixed, specified angle. Surface wave overlay transducers with their more complicated field structure use other piezoelectric coefficients also, and constitute an even more stringent test of a film.

The value of k for a bulk, longitudinal transducer has been measured in this study by fabricating a one-port bulk delay line with a ZnO film of known thickness and orientation. Above and below this film are electrodes of known material, thickness, and area, and this whole assemblage is in turn mounted on a substrate of known surface smoothness, surface parallelism, propagation loss, propagation anisotropy, and orientation. Knowing these parameters, we can calculate k from measurements of the untuned insertion loss vs frequency. Two other useful techniques involve measurement of the transducer's input impedance vs frequency, and of the transducer's impulse response vs time. Both require knowledge of just as many parameters and are generally not as accurate or convenient. The latter, however, does give additional phase information.

Resistivity

The RF electric field across a ZnO film must produce negligible conduction current. Making series $R = \rho (t/A) > 10^4 \Omega$ for a 10-GHz bulk wave transducer requires a resistivity $\rho > 4 \times 10^4 \Omega \text{ cm}$ (for a film thickness $t = 0.3 \mu\text{m}$ and 5-mil-diam top dot (area = A)).

Optical Quality

Clear films, as opposed to cloudy, appear to give better k 's and higher resistivities. Clear films seem to consist of smaller, more uniform, and more densely packed crystallites with consequently less surface irregularity.

Microstructure, SEM Photographs

Carbon-coated ZnO films can be analyzed using scanning electron microscope (SEM) photographs. Considerable recent work has been done in trying to correlate electrical performance with microstructure of the film surface and along a cleaved film edge. Figure 1 shows some examples. A smooth, densely packed (on a 0.1- μm scale) structure seems to give better performance for surface wave generation. It seems questionable

whether roughness on a scale much greater than 0.1 μm could be tolerated for 0.3- μm -thick X-band transducer films.

Electron Diffraction

Structure within a few atomic layers of the ZnO surface is revealed by electron diffraction, giving some indication of crystallite orientation. Alignment problems and surface preparation make this a more difficult procedure than several types of x-ray analysis.

X-ray Analysis

The greatest difficulty in using x-ray techniques on these films is the relatively low stopping power of zinc and oxygen together with the small film thickness to be analyzed. Scattering from counterelectrode layers (gold has a large stopping power and is a common counterelectrode) and especially the substrate, even an amorphous substrate, quickly obscures any return from the ZnO film, but these techniques can still provide valuable information.

Laue backscatter photographs taken on several good samples (ZnO/Au/Al₂O₃) were strongly obscured by the Al₂O₃ pattern, and were hazed out in another case by uniform substrate scattering with a fused quartz substrate.

The same 0.7- μm ZnO on a fused quartz sample was scanned with a proportional counting x-ray diffractometer using copper radiation. The count rate is plotted vs 2θ (where θ is the scattering angle) in Fig. 2, which shows the resulting ZnO peak. An expanded trace from the 28° to 38° range of 2θ is included. The diffractometer scan intensity gives only a rough measure of the proportion of ZnO with c axes exactly (to within instrument resolution) normal to the substrate surface. X rays scattered from crystallites with c axes slightly tilted from normal would not be detected. The strong peak at $\theta = 17.5^\circ$ ($2\theta = 35^\circ$) corresponds to the correct ZnO basal plane (showing at least some c axes normal), and its angular width gives an indication of crystallite size. A value of $S \approx 100 \text{ \AA}$ is estimated by using

$$S = K \lambda (\Delta^2 - \Delta_o^2)^{-1/2} (\cos\theta)^{-1}, \quad (1)$$

where

S is a mean crystallite diameter

$\lambda = 1.54 \text{ \AA}$ is the x-ray wavelength

K is a constant about 1.0

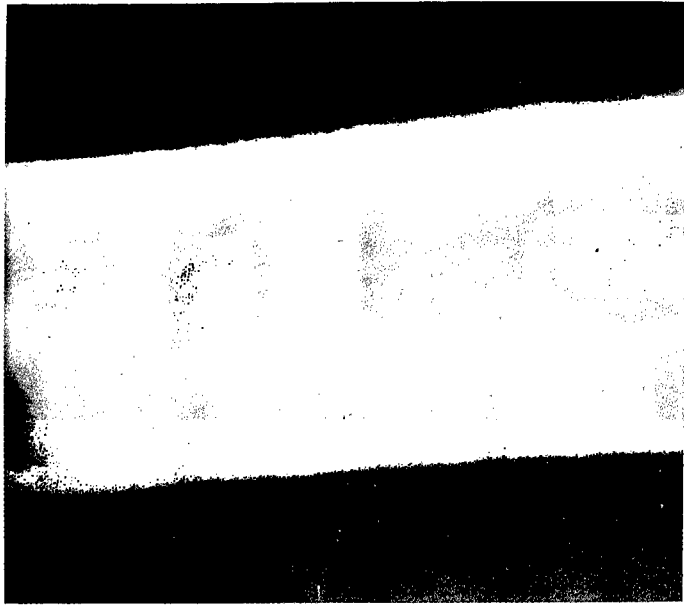
θ the Bragg scattering angle of 17.5°

$\Delta_o = 0.20$, the given angular resolution of the diffractometer

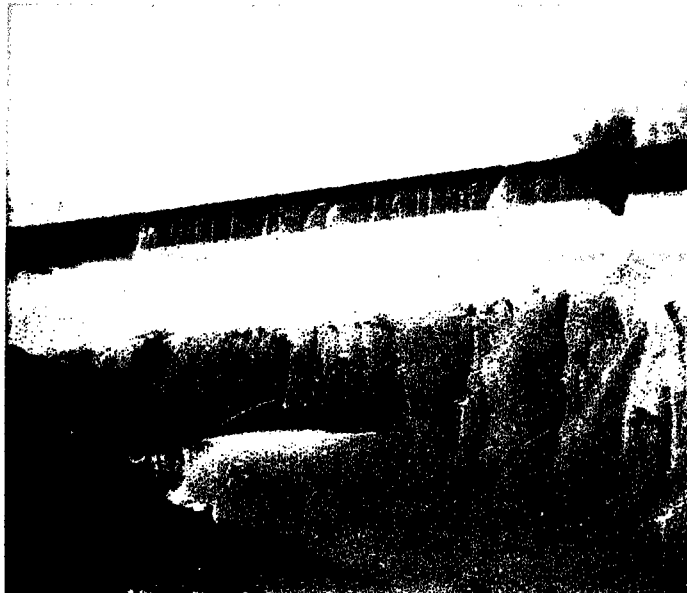
$\Delta = 0.8^\circ$, the angular width of the scattered peak from Fig. 2.

A factor of 4 error in Δ_o , e.g. caused by collimator slit canting, would extend the estimate of S to infinity. Small, oriented crystallites (small S) usually mean better film properties.

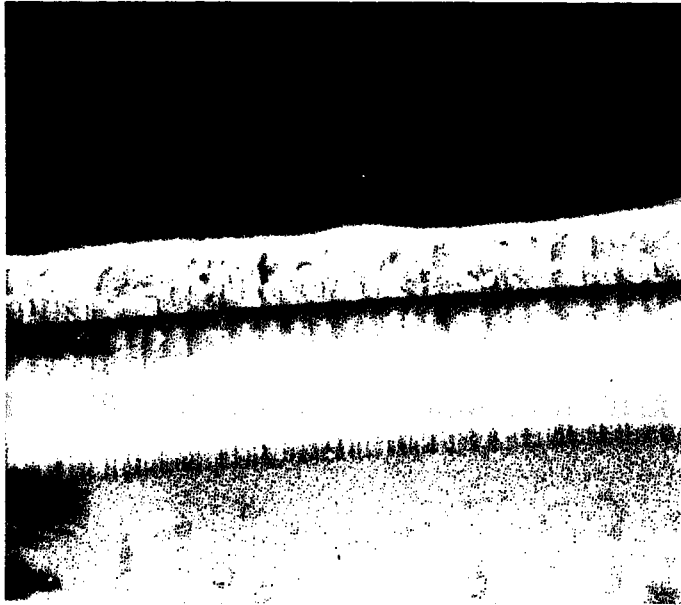
LARSON AND FINNLEY



(a) $(10.4 \times 10^3) \times$



(b) $(2.0 \times 10^3) \times$



(c) $(2.0 \times 10^3) \times$



(d) $(10.4 \times 10^3) \times$

Fig. 1 — Scanning electron microscope photographs
(Hickernell ZnO film)

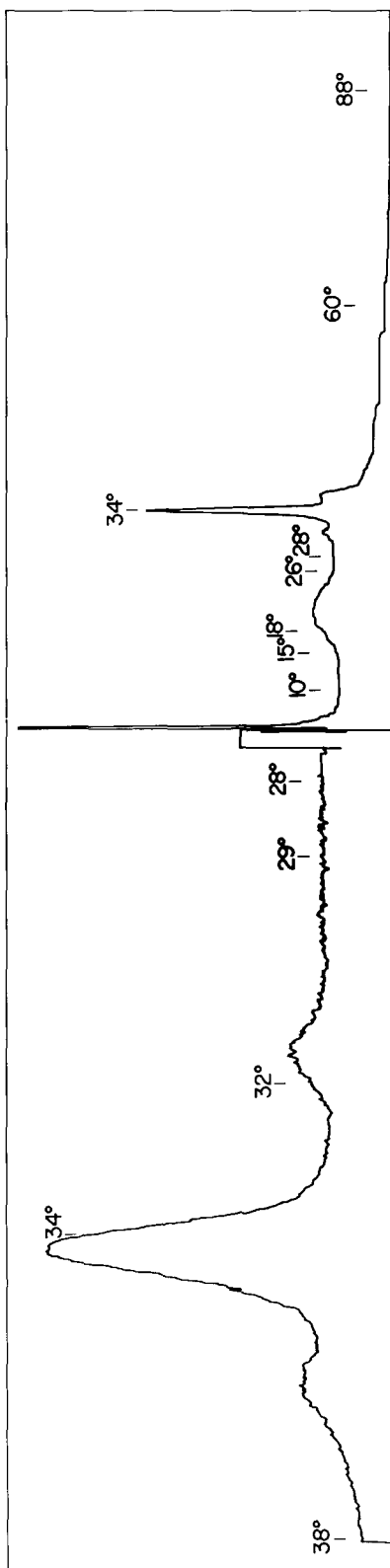


Fig. 2 — Diffractometer scan

A Debye Scherrer camera picture, with 17.5° incidence angle, would give the same information as the diffractometer scan, plus an estimate of c axis misalignment about one axis lying in the film plane. A rocking curve, where the sample is rocked about the ZnO basal plane angle keeping the source and angle of detection fixed, would give a precise measure of misalignment about one axis. Good transducer performance has been observed for rocking angle widths up to 20° .

BULK WAVE TRANSDUCER ANALYSIS

The basic configuration of a delay line excited by a bulk wave piezoelectric transducer is shown in Fig. 3. A two-port delay line has an identical transducer aligned at the other end of the delay medium, while in a one-port line the pulsed signal is reflected from a polished parallel end face and detected by the generating transducer after two transits. Total time delay is determined by the delay medium length and sound velocity. Specific properties of materials used in this study (sound velocities, attenuations, and acoustic impedances) are listed in Table 1.

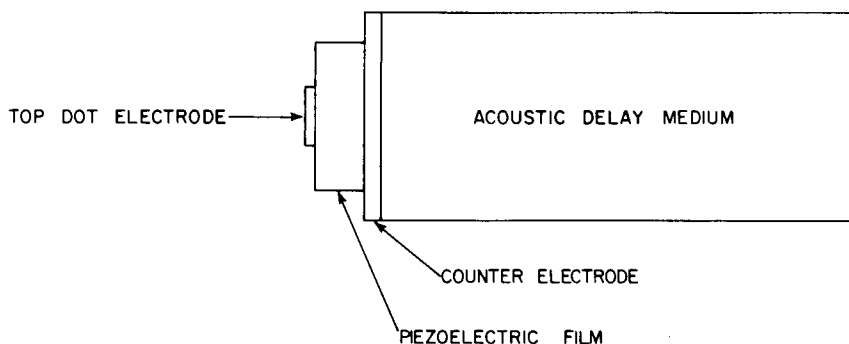


Fig. 3 — Basic transducer configuration

The main advantage of working at microwave frequencies rather than at VHF or UHF is the greater bandwidth obtained. The main disadvantages are fabrication difficulty and insertion loss. Indeed, insertion loss is the Achilles heel of devices operating at these frequencies. Possible contributions to insertion loss and a discussion of their causes follows:

Matching or reflection loss occurs due to the difficulty of making the transducer input impedance match that of the transmission line feed. Because of symmetry, the match that the returning pulse sees in the other direction is just as bad, causing most of the power to be reflected and hindering detection of the returning pulse. Included in this category is ohmic loss in any matching network. This problem will be considered in detail later.

Diffraction loss occurs because the generated acoustic beam spreads to an area greater than the receiving transducer. A criterion to determine that this is a problem is

$$\frac{\lambda}{D} > \frac{D}{L} \quad (2)$$

where

λ is the acoustic wavelength

D is the active area diameter

L is the total acoustic propagation length.

Table 1
Important Physical Constants*

Material	Propagation Direction	Mode	k	ϵ_s/ϵ_o	V_o (10^3 m/s)	Z_o 10^6 kg/m ² s
ZnO	Z	Long	0.28	8.8	6.33	36.0
	X	Shear	0.32	8.3	2.72	15.5
Al ₂ O ₃	Z	Long	—	—	11.1	44.3
	Z	Shear	—	—	6.04	25.2
Au	[100]	Long	—	—	3.21	61.3
	[100]	Shear	—	—	1.47	28.4
Al	[100]	Long	—	—	6.35	17.2
	[100]	Shear	—	—	3.25	8.8

*Data from Ref. 2, Table I and II.

There are two categories of *misalignment loss*. *Nonparallelism* of the generating and receiving active areas causes the received acoustic phase front to be tilted with respect to the receiving area with subsequent signal cancellation. An example of a one-port echo pattern caused by nonparallelism is shown in Fig. 4. In this case, nonparallelism is caused by misalignment of the parallel faces of the delay medium. *Lateral Displacement* of the received beam means that it misses the receiving transducer by some amount. This alignment problem is tougher in a two-port device. Both problems are accentuated by an anisotropic delay medium, which may exhibit beam "walk-off" when the phase and group velocities are not colinear. Sapphire is anisotropic and exhibits beam walk-off for most propagation directions, but specifically not for longitudinal wave propagation exactly along the c axis. Crystal alignment (i.e. keeping the c axis exactly normal to the polished faces) is very important for this material.

Medium loss is attenuation suffered by the propagating acoustic wave in the transmission media. It is characterized by an f^2 dependence at room temperature. See Table 1 for sapphire loss data. Losses in the delay medium are usually much greater than in either

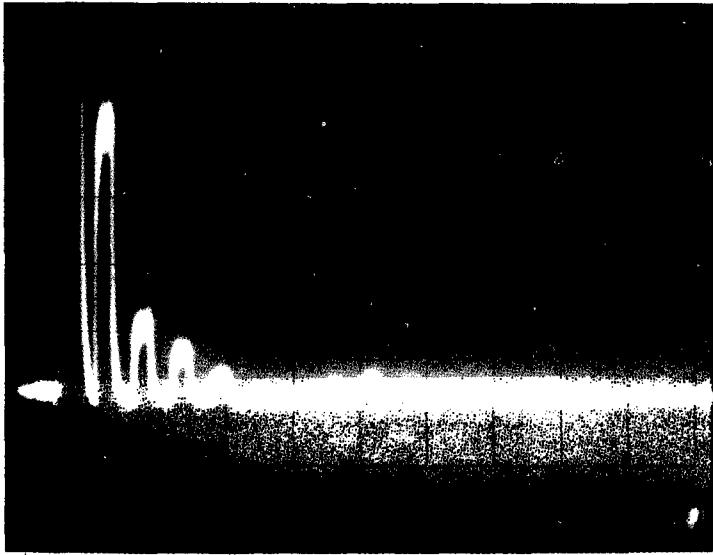


Fig. 4 — Nonparallel echo pattern

the active film or the electrodes because of the relative path lengths, though medium loss in the active layer can become appreciable at high power levels or under high acoustic Q tuning using matching layers.

Matching considerations can be illustrated using the equivalent circuit in Fig. 5, valid at the center frequency of a transducer pass band. The more complicated Mason equivalent circuit gives an excellent description of transducer behavior, and is covered thoroughly in Ref. 2.

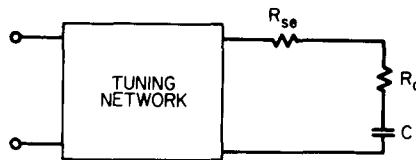


Fig. 5 — Equivalent circuit

Consider first the untuned case, where the tuning network in Fig. 5 is omitted, and R_{se} is the series ohmic contact resistance of the transducer mount. The loss ratio T is defined by

$$T = \frac{P_A}{P_L}$$

where P_A is the power available from the source under matched conditions and P_L is the power absorbed by R_A , i.e., radiated as bulk waves. Then from Fig. 5,

$$T = \frac{(Z_o + R_{se} + R_A)^2 + (1/\omega_o C_o)^2}{4 Z_o R_A} \quad (3)$$

at ω_o or midband. From Ref. 2, the radiation resistance R_A is found to be

$$R_A = \frac{4 k^2 Z_{\text{sapphire}}}{\pi Z_{Zno}} \frac{1}{\omega_o C_o} \quad (4)$$

For R_{se} , $R_A \ll Z_o$ (Z_o is typically 50Ω); using Eqs. (3) and (4) and setting the derivative with respect to $1/\omega_o C_o$ equal to zero, we find that minimum untuned loss occurs for $1/\omega_o C_o = Z_o$. This determines top dot area A since ϵ (dielectric constant) and t (film thickness) in

$$C_o = \epsilon A/t \quad (5)$$

are determined by material and operating frequency, respectively.

Untuned insertion loss measurements are important because all of the quantities in Eqs. (3) and (4) are known or can be measured except k and R_{se} , which may vary from mount to mount. But in Eq. (3) R_{se} can be neglected compared to Z_o . Thus Eq. (3) gives a good method of measuring k , and the untuned conversion loss depends primarily on k (i.e., on how good a film has been grown).

Tuned insertion loss, the main performance parameter for a practical device, depends critically on a tuning network and contact losses (represented by R_{se} in Fig. 5) as well as on the film k . Making $R_A = 50 \Omega$ (to match Z_o) becomes impractical for frequencies much above 1 GHz. At 1 GHz, using $k^2 = 0.05$ in Eqs. (4) and (5) and setting $R_A = 50 \Omega$ gives $D \approx 5$ mils ($D =$ top dot diameter). This results in considerable diffraction loss which would get worse as frequency increases, if R_A is to remain constant.

At a single frequency, the minimum tuned insertion loss is

$$\frac{R_A}{R_A + R_{se}} \quad (6)$$

Typical numbers at X-band are (using $k^2 = 0.05$, $D = 6$ mils, $R_{se} = 1 \Omega$):

$$\frac{1}{\omega_o C_o} = 4 \Omega \text{ at } 10 \text{ GHz, } R_A = 0.32 \Omega, R_A / (R_A + R_{se}) = 0.25, \quad (7)$$

or 6dB of insertion loss. A simultaneous match for both electric and acoustic zero reflection is not possible for $R_{se} > 0$. This is important where two-port delay lines are concerned, since the third reflection (caused by a bad match) returns the wave to the output, but delayed by the triple transit time. One would like to minimize this reflection. Note that k enters the expression for R_A squared, so performance deteriorates rapidly for poorer films. R_A is maximized by growing good films; R_{se} is minimized by good top dot contacting methods and low loss (e.g., electrically short) tuning networks.

For broadband tuned operation, the acoustic Q of the bulk wave transducer is a vital factor;

$$Q_{\text{acoustical}} = Q_A = \frac{1/\omega_o C_o}{R_A} \quad \text{or} \quad \frac{1}{k^2} \quad (8)$$

or $Q \geq 20$ for ZnO on the average. Neglecting the tuning network, electrical Q , and R_{se} (this is not usually a good assumption—numbers derived will be idealized), we can use a theorem from network analysis to estimate Γ_{\min} , the minimum voltage reflection coefficient achievable for a desired fractional bandwidth W ;

$$\ln \left| \frac{1}{\Gamma_{\min}} \right| = \frac{\pi}{WQ} \quad (9)$$

Using $W = 0.5$ and $Q = Q_{\text{acoustical}} = 20$ gives $\Gamma_{\min} = 0.73$, or $VSWR_{\min} = 6.4$, or 3.3 dB of one-way transmission loss that cannot be avoided.

The choice of sapphire and ZnO materials was also made because their acoustic impedances match quite well: $Z_{\text{sapphire}}/Z_{\text{ZnO}} = 1.25$ (see Table 1). However, combinations of materials with greater degrees of mismatch can be utilized and insertion loss improved (at the cost of bandwidth) by the use of additional intermediate, inactive, impedance-transforming layers usually placed beneath the counterelectrode. The gain-bandwidth product is generally reduced and losses in the transducer are increased.

Counterelectrodes should be acoustically thin, i.e., much less than one-half acoustic wavelength thick. For gold films at X-band, however, conductivity would suffer. The 1700-Å thickness chosen is one-half the acoustic wavelength at 10 GHz. The predicted effect on insertion loss in the production of a symmetric ripple, about f_o , of 3 dB or less across the band. Thicker layers would introduce asymmetric ripple, slightly more severe.

Top dot acoustic thickness is much more critical than counterelectrode thickness. A related problem is an inactive ZnO layer which can grow on top of the active portion. Reference [9] thoroughly treats these problems, and only results will be given here. Poles (frequencies at which the loss becomes infinite) are introduced by thick top electrode layers. The pole frequencies are solutions of:

$$\begin{aligned} & (\sin 1/2 \theta_o) [(1 + r_1) \sin \frac{\theta_o}{2} (1 + 2d_1) \\ & + (1 - r_1) \sin \frac{\theta_o}{2} (1 - 2d_1)] = 0, \end{aligned} \quad (10)$$

where

$$\theta_o = \pi f / f_o,$$

$$r_1 = Z_{\text{top dot}} / Z_{\text{active layer}}$$

$$d_1 = \text{acoustic thickness of the top layer } (d_1 = 1.0 \text{ for a layer half a wavelength thick}).$$

The first term describes the pole at the active-layer full-wave frequency $f = 2f_o$. The practical import of the second term is to keep d_1 less than 0.1, i.e., keep the top electrode thickness less than 0.05 acoustical wavelength. Aluminum, with twice the longitudinal sound velocity of gold, is thus a good choice for a top dot material. Even so, the 0.05λ criterion above implies 300-Å-thick aluminum top dots at 10 GHz, and a severe conductivity problem at higher frequencies (because even thinner dots are required).

The inactive layer problem is treated by setting $r_1 = 1$ in Eq. (10). Solving for the first pole gives

$$f_{\text{pole}} = \left(\frac{v}{2t} \right) \frac{2t}{t + t_i}$$

where

$$t = t_i + t_a = \text{total ZnO thickness}$$

$$t_i = \text{thickness of the inactive layer}$$

$$t_a = \text{thickness of the active layer.}$$

The midband frequency is $v/2t$ for no inactive layer. Note that as $t_i \rightarrow t$, the first loss pole approaches $v/2t$ from above. The full wave pole at v/t for no inactive layer is simultaneously pushed up to a value v/t_a .

TECHNIQUES

Radio-frequency diode sputtering was chosen as the method of growing ZnO active films. Other methods have been successful for bulk wave transducers below 2 GHz: two-source evaporation, reactive evaporation of Zn in an oxygen atmosphere, dc diode reactive sputtering of Zn in an oxygen atmosphere, dc diode sputtering of ZnO, dc triode sputtering of ZnO, and vapor phase epitaxy. The easiest to control seemed to be RF diode sputtering; it has the greatest flexibility in deposition parameters, and has been used successfully by others [10, 11]. The easy availability of equipment was also a factor in selecting this method.

The following sputtering parameters were found to work for X-band ZnO transducers:

RF power: 200 W

Self bias voltage: 800 V

Pressure: 9 μm of 80/20 Ar₂/O₂ mixture

Rate: 0.6 to 0.7 $\mu\text{m/hr}$

Target-substrate separation: 2.5 in.

Target diameter: 5 in.

An MRC 8622 sputtering system was used, pumped by an LN₂ trapped 6 in. diffusion pump, which was throttled during sputtering to keep the fore-pressure within acceptable limits. Overnight sample bake-out at deposition temperature gave a base pressure of 5 to 8 $\times 10^{-7}$ torr.

Thickness was monitored optically using the setup illustrated in Fig. 6. Chopping the incident 6328 Å light at 360 Hz and using a phase-locked amplifier reduced sensitivity to plasma luminosity fluctuations. θ_1 was about 20°. Maximum interference contrast between maxima and minima was obtained by aligning the incident light E-field polarization direction in the plane of incidence. With this orientation, and for $\theta_1 <$ Brewster's angle, the other component is not reversed in phase when reflected at the dielectric-vacuum interface. A trace of detected chopped light intensity vs time is shown in Fig. 7. The thickness interval between minima is

$$\Delta t = \frac{\lambda_{\text{light}}}{2 (n^2_{\text{ZnO}} - \sin^2 \theta_1)^{1/2}} \quad (12)$$

Calibration using a Toulanski thickness measurement method gave $\Delta t = 0.18 \mu\text{m}$ or $n_{\text{ZnO}} = 2.0 \pm 10\%$ which agrees with the bulk value of 2.003.

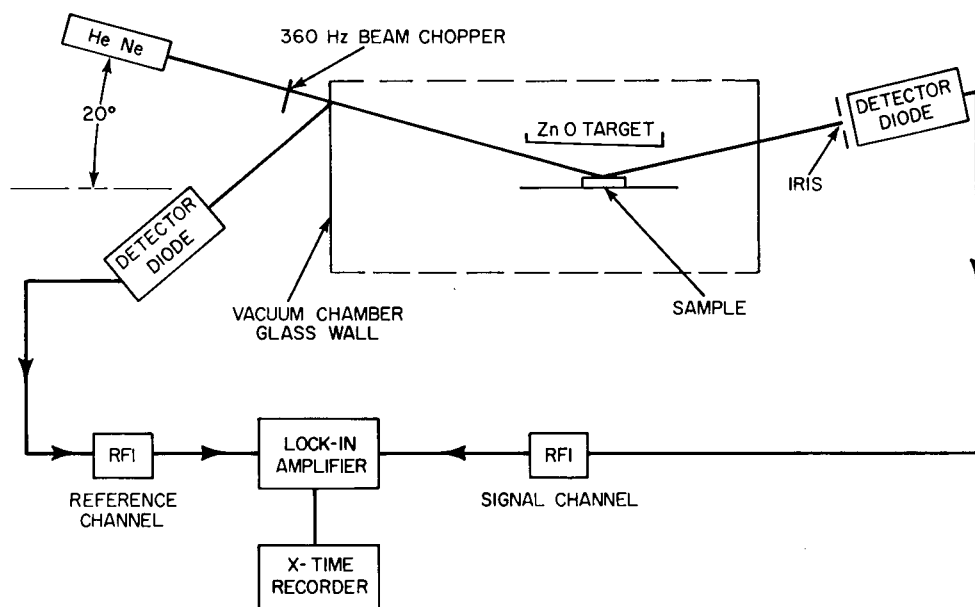


Fig. 6 — Laser monitor setup

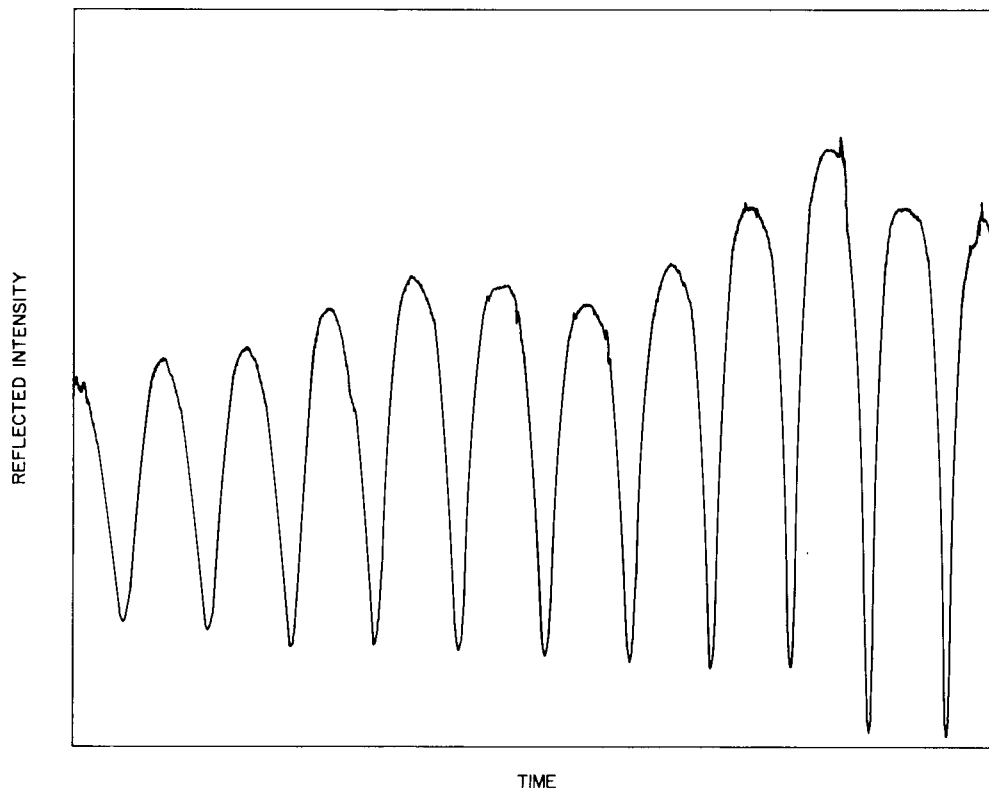


Fig. 7 — Laser monitor output trace

A total Cr-Au thickness of 1700 \AA on a polished 1/2-in.-diam by 1/4 in.-thick sapphire (c axis normal to faces) was evaporated in another system. Various cleaning procedures including hot NaOH, hot chromic acid, and isopropyl alcohol vapor were tried on these counterelectrode films, but the best results were obtained merely by keeping the samples very clean after the gold evaporation. Heat sinking the sample was very important, and various configurations were tried. The best one is illustrated in Fig. 8 with the addition of a little liquid gallium metal to provide intimate thermal contact between heat sink and sapphire.

Delay-line fabrication and mounting was done as follows: after deposition, the central portion of the uniform ZnO layer was masked off with black wax dissolved in trichloroethylene, leaving a 1-mm strip around the circumference. ZnO was removed from this region using a 1:1 phosphoric acid/water etch, leaving the gold. After removing the black wax with trichloroethylene, the sample was mounted in a brass ring holder using Duco Cement. Aluminum top electrodes (dots) were evaporated through a 3-mil-thick molybdenum mask having 5.9-mil holes on 15-mil centers for X-band, and 11.2-mil holes on 30-mil centers for L-band. This gave several dozen transducers per run, which was very helpful in view of poor contacts, contact punch-through, and particles on films. It served also as a check on performance uniformity over the entire film area.

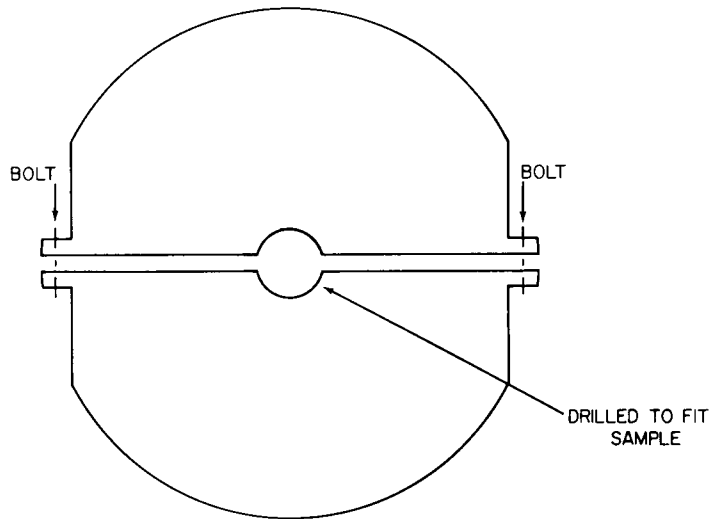


Fig. 8 — Heat sink configuration

Using the same brass holder, samples were electrically mounted using indium gaskets to contact the ZnO-free borders of the gold film and provide ground contact. Two examples of electrical mounts used are shown in Figs. 9 and 10. The best electrical and mechanical top dot contacting method utilized commercial spring-loaded contacts (pogo sticks) with rounded tips and 20-mil travel.

RESULTS AND PROBLEMS

Figure 11 shows untuned insertion loss data on a *c* axis sapphire, one-port delay line with the following thicknesses: top dot, $0.1\ \mu\text{m}$ Al; active film, $1.8\text{-}\mu\text{m}$ ZnO; counter-electrode, $0.17\text{-}\mu\text{m}$ Cr-Au. Calculated from these data, k is 0.16, compared to a bulk value of 0.28. The total round-trip loss in the sapphire (medium, misalignment, and diffraction loss) was estimated from subsequent echoes as 4dB. A narrowband measurement with the transducer tuned to one frequency, using coaxial stub tuners, is illustrated also. Comparable performance has been obtained on other lines.

Figure 12 shows data on an X-band one-port line. Layer thicknesses were $0.1\ \mu\text{m}$ Al, $0.34\ \mu\text{m}$ ZnO, and $0.17\ \mu\text{m}$ Cr-Au. Again the second echoes give an estimate of total nontransducer losses. Variable microstrip tuning, using indium foil and the mount shown in Fig. 10, was not very successful. The best insertion loss over the band was approximately equivalent to the untuned data shown in Fig. 12. The coaxial untuned mount in Fig. 9 probably had some effective series inductance, but the main reasons for poor microstrip mount performance at X-band were ohmic loss in the indium foil and radiative loss in the microstrip mount. These, in effect, made R_{se} too large in the equivalent circuit model.

LARSON AND FINNLEY

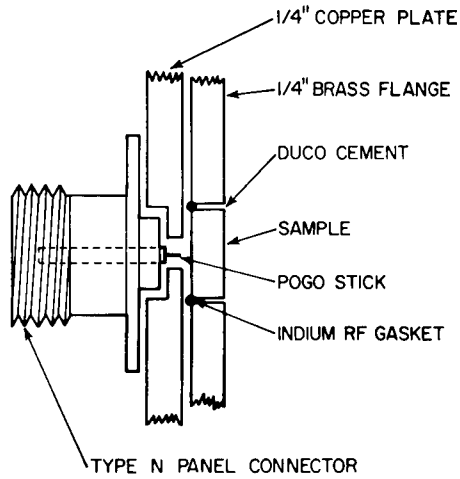


Fig. 9 — Coaxial mount

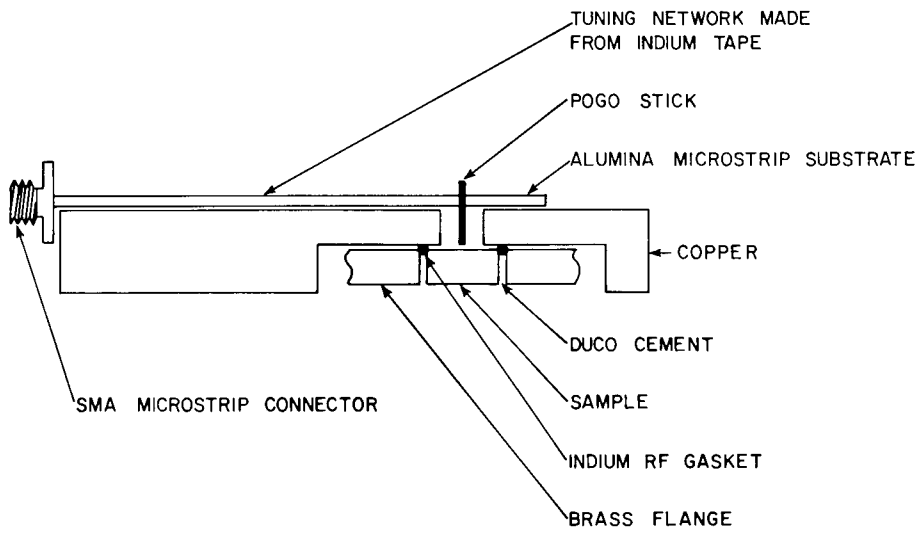


Fig. 10 — Microstrip mount

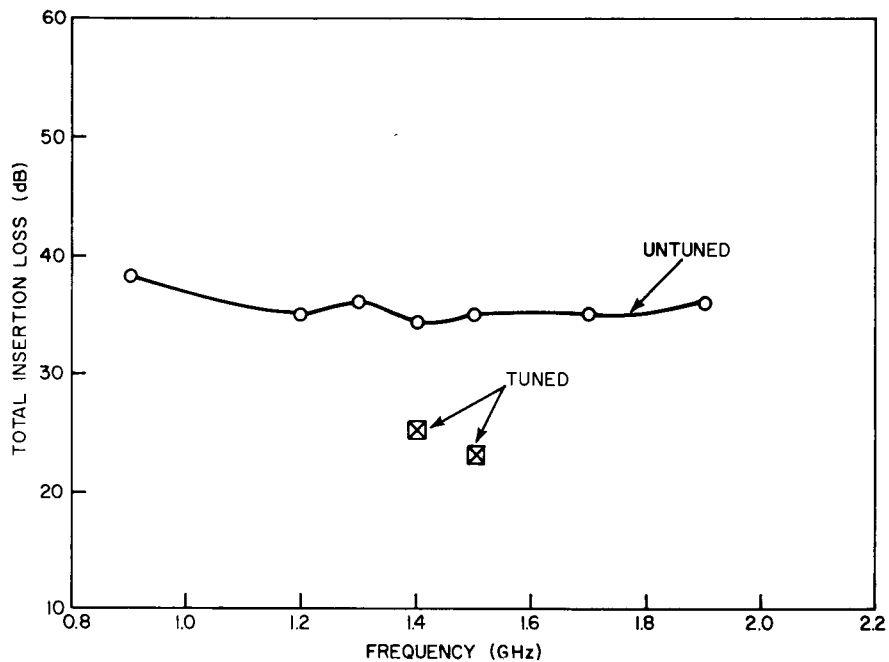


Fig. 11 — Insertion loss, 1-2 GHz bulk wave delay line

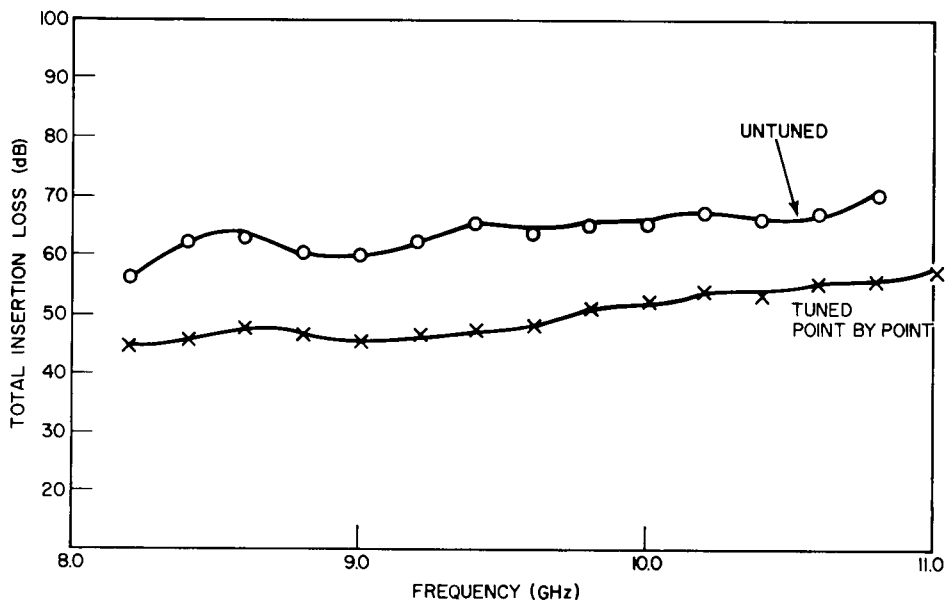


Fig. 12 — X-band data

The main problem encountered in the sputtered zinc-oxide films was the growth of inactive layers, described earlier, on top of the films. Untuned insertion loss data on a 0.1- μm Al/2.2- μm ZnO/0.17- μm Ti-Au sapphire one-port line is shown in Fig. 13. In this severe case, inactive layer theory indicates that almost the entire ZnO layer is inactive, since the pole is pushed down almost to the theoretical midband point. Thin X-band layers never exhibited this problem. The reasons for the growth of dead layers are not well understood, but the best educated guesses point to contamination during a run or inadequacies in the gold counterelectrode layer. These dead layers are comparable to those observed by others using similar methods.

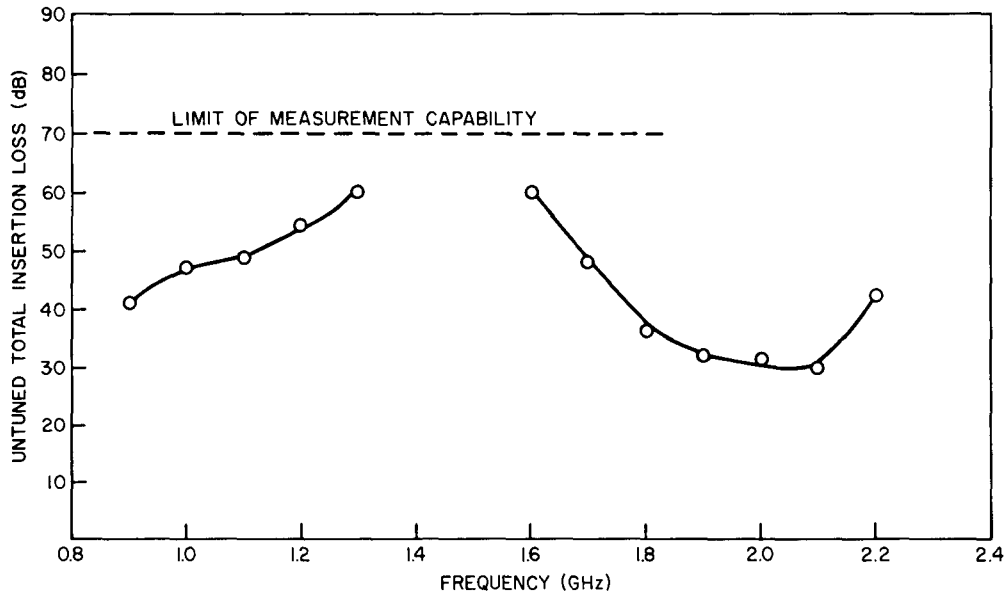


Fig. 13 — Insertion loss of a 1-2 GHz bulkwave delay line showing a pole

One other type of acoustic delay device was attempted: the so-called overlay or interdigital surface wave transducer. Figure 14 illustrates this type of acoustic surface wave (ASW) transducer. Figure 15 is a picture of an actual device fabricated at NRL. The substrate is a 3/4-in.-diam fused quartz optical flat on which are fabricated 12 aluminum interdigital transducers with these dimensions:

- Finger width = 3.05 μm
- Width/gap ratio = 1.0
- Number of finger pairs = 20
- Overlap length = 0.75 mm
- Separation = 0.100 in.
- (ASW path length)

Most transducers gave comparable performance except for those with missing fingers. The following data are representative:

ZnO layer thickness d	= 4.8 μm
d/λ	= 0.4
ASW phase velocity (agrees with Ref. 12)	= 2.6×10^3 m/s
Center	= 220 MHz
Bandwidth	= 5%
Untuned total insertion loss between adjacent transducers	= 55 dB
Series L tuned insertion loss between adjacent transducers	= 39 dB
ASW propagation loss between two adjacent transducers	= 4 dB
Total measured capacitance	= 1.8 pF
Theoretical transducer capacitance (see Ref. 11)	= 1.5 pF

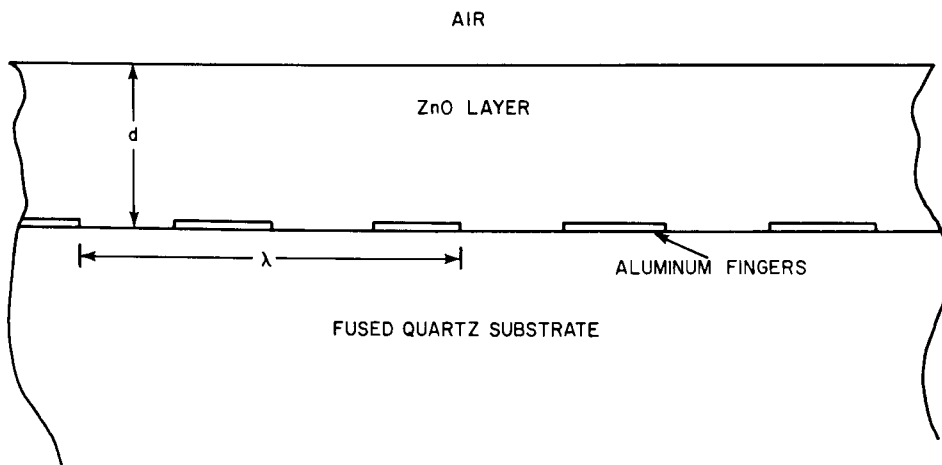


Fig. 14 — Overlay ASW transducer diagram



Fig. 15 — Picture of overlay transducer

A bulk wave transducer grown simultaneously exhibited a dead layer, and predictably, the overlay performance gave a value of approximately 1% of the theoretical value of k^2 [11]. This performance probably indicates the presence of a dead layer in this zinc oxide film also. Further work to eliminate these layers is in progress.

FUTURE OUTLOOK

Practically, one would like to push bulk wave delay lines to higher frequencies with decreased insertion loss. Intrinsic attenuation in most delay media can be reduced at least by a factor of 10 by cooling to cryogenic temperatures.

Intrinsic loss within the transducer could also be reduced, but this is not a major contribution to insertion loss. At frequencies much above X-band, top dot loading would become severe. A necessary compromise would be to live with the insertion loss pole brought on by this loading, markedly reducing the usable bandwidth.

Several methods have been proposed to improve the bulk wave transducer matching problem. Parallel inductors fabricated very close to the active region by cleverly designing the counterelectrode would reduce R_{se} . Series connection of metal and active layers by physically stacking them increases the effective total radiation resistance R_A but reduces bandwidth proportionally. The same bandwidth reduction occurs in devices with successive active layers having alternating polarities, or with alternating inactive layers one-half wavelength thick of some insulator. Series connection of several transducers in the same plane would increase R_A and keep the same bandwidth, but the interconnection problem is difficult, and the resulting bulk wave radiation pattern must be carefully analyzed. Also, configuration with nonuniform thicknesses or electric fields have not been well analyzed.

Finally, since achievable gain-bandwidth products depend on k^2 , a search could be made for growable active films with higher values of k . Lithium niobate, for example, has a bulk longitudinal k of 0.5, but has not yet been grown as an active thin film.

The ability to make good bulk transducers implies a capability for making reproducibly good zinc oxide films (no small achievement in itself), which can also be used to generate acoustic surface waves on other than piezoelectric materials. In fact, the fabrication of these surface wave, or overlay, devices served as primary motivation for the foregoing work. One such interdigital overlay transducer, illustrated in Fig. 14, is similar to the one attempt previously mentioned in this paper. The quality of the zinc oxide film, again, is very important, and the evaluation of a bulk transducer grown simultaneously with the overlay transducer serves as a convenient indicator of that quality.

ACKNOWLEDGMENTS

The authors are grateful to Dr. A. Bahr (Stanford Research Institute) who provided the SEM photographs, and B. N. Schmidt, Code 5214, for use of the x-ray diffractometer.

REFERENCES

1. L. R. Whicker, P. F. Garcia, and G. E. Evans, IEEE Trans. Microwave Theory Tech. MTT-15, 755 (Dec. 1967).
2. T. M. Reeder and D. K. Winslow, IEEE Trans. Microwave Theory Tech. MTT-17, 927 (1969).
3. G. E. Evans, "Piezoelectric Transducers for Microwave Ultrasonics" (Ph.D. dissertation, University of Maryland, 1967).
4. M. T. Wauk, "Attenuation in Microwave Acoustic Transducers and Resonators" (Ph.D. dissertation, Stanford University, 1969).
5. R. M. Malbon, "Acoustic Generation with Reactively Deposited Piezoelectric Thin Films" (Ph.D. dissertation, Stanford University, 1969).
6. J. D. Larson, "Acoustic Wave Generation by Piezoelectric Plates and Films" (Ph.D. dissertation, Stanford University, 1971).
7. N. F. Foster, et al., IEEE Trans. Sonics Ultrasonics SU-15, 28 (1968).
8. J. D. Larson, et al., IEEE Trans. Microwave Theory Tech. MTT-18, 602 (1970).
9. J. D. Larson, et al., IEEE Trans. Sonics Ultrasonics SU-19, 18 (1972).
10. A. H. Fahmy and E. L. Adler, IEEE Trans. Sonics Ultrasonics SU-19, 346 (1972).
11. F. S. Hickernell in *Acoustic Surface Wave and Acousto-Optic Devices*, Thomas Kallard, editor, Optosonic Press, New York, Sept. 1971.
12. V. A. Polotmyagin and V. N. Shevchik, "Theory of Excitation of Microwave Elastic Waves by Miltifilm Transducers," in *Radio Engrg. Electron. Phys.* 17, 978 (June 1972), English translation.